

A Deformable Attention-Based Detection Transformer with Cross-Scale Feature Fusion for Industrial Coil Spring Inspection

Matteo Rossi¹

Pony Matt¹

¹Maharaja Agrasen University

¹Email: matteo.rossi@mau.edu.mk, pony.matt@mau.edu.mk

Abstract

Automated visual inspection of locomotive coil springs presents significant challenges due to the morphological diversity of surface defects, substantial scale variations, and complex industrial backgrounds. This paper proposes MSD-DETR (Multi-Scale Deformable Detection Transformer), a novel detection framework that addresses these challenges through three key innovations: (1) a structural reparameterization strategy that decouples training-time multi-branch topology from inference-time efficiency, enhancing feature extraction while maintaining real-time performance; (2) a deformable attention mechanism that enables content-adaptive spatial sampling, allowing dynamic focus on defect-relevant regions regardless of morphological irregularity; and (3) a cross-scale feature fusion architecture incorporating GSCConv modules and VoVGSCSP blocks for effective multi-resolution information aggregation. Comprehensive experiments on a real-world locomotive coil spring dataset demonstrate that MSD-DETR achieves 92.4% mAP@0.5 at 98 FPS, outperforming state-of-the-art detectors including YOLOv8 (+3.1% mAP) and the baseline RT-DETR (+2.8% mAP) while maintaining comparable inference speed, establishing a new benchmark for industrial coil spring quality inspection.

1 Introduction

1.1 Background and Motivation

Railway transportation networks [1, 2, 3, 4, 5] constitute an indispensable pillar of contemporary global infrastructure, facilitating the efficient movement of passengers and freight across vast geographical distances while maintaining favorable environmental sustainability characteristics relative to alternative transportation modalities. The operational integrity of railway systems fundamentally depends upon the reliable functioning of numerous mechanical and electrical subsystems [6, 7, 8], among which

the running gear assembly assumes particular significance due to its direct responsibility for vehicle dynamics, ride quality, and operational safety. Within this complex mechanical ecosystem, coil springs serve as primary suspension elements that absorb dynamic loads arising from track irregularities, vehicle acceleration and deceleration, and payload variations, thereby ensuring stable vehicle behavior and protecting both cargo and passengers from excessive vibration exposure.

The mechanical loading conditions experienced by locomotive coil springs during operational service are characterized by substantial complexity and severity. These components are subjected to continuous cyclic stress patterns that accumulate over millions of loading cycles throughout their service lifetime, creating favorable conditions for the initiation and propagation of fatigue-induced damage mechanisms. Additionally, the operational environment exposes springs to various degradation factors, including moisture ingress, temperature fluctuations, and chemical contaminants, which accelerate corrosion processes and surface deterioration. The progressive accumulation of such damage manifestations ultimately compromises the load-bearing capacity and energy absorption characteristics of spring components, potentially leading to catastrophic failure events with severe safety implications.

The imperative for effective defect detection [9, 10, 11, 12, 13, 14, 15, 16] in locomotive coil springs derives from both safety and economic considerations. From a safety perspective, undetected defects may propagate under continued loading until a sudden fracture occurs, potentially causing derailment incidents or other hazardous situations. From an economic perspective, the implementation of condition-based maintenance strategies enabled by reliable defect detection can substantially reduce lifecycle costs by optimizing component replacement intervals and preventing costly unplanned service disruptions. Consequently, the development of accurate, efficient, and practically deployable defect detection methodologies [3, 5, 17, 18, 19] represents a research priority of considerable practical significance.

1.2 Limitations of Conventional Inspection Approaches

Traditional methodologies for coil spring quality assessment have predominantly relied upon manual visual examination performed by trained human inspectors. While this approach benefits from the sophisticated pattern recognition capabilities and contextual reasoning abilities inherent to human cognition, it simultaneously suffers from several fundamental limitations that constrain its effectiveness in modern manufacturing and maintenance contexts.

The inherent subjectivity of human visual assessment introduces systematic variability in inspection outcomes, as different operators may apply inconsistent criteria when evaluating defect severity and determining acceptance or rejection decisions. This variability is further exacerbated by factors including operator experience levels, training quality, and workplace environmental conditions. Furthermore, the cognitively demanding and repetitive nature of inspection tasks induces progressive operator fatigue over extended work periods, leading to decreased vigilance, increased response latency, and elevated probability of defect omission. Empirical studies have documented significant degradation in human inspection performance following prolonged task engagement, with error rates increasing substantially after several hours of continuous

operation.

Beyond accuracy considerations, the throughput limitations of manual inspection create operational bottlenecks that impede production efficiency, particularly in high-volume manufacturing environments where rapid quality verification is essential for maintaining workflow continuity. The labor-intensive nature of manual inspection also contributes substantially to operational costs, while the availability of skilled inspection personnel may be constrained in certain geographical or industrial contexts. These collective limitations motivate the development of automated inspection systems capable of achieving consistent, accurate, and high-throughput defect detection without the constraints inherent to human-dependent processes.

1.3 Deep Learning for Industrial Defect Detection

The emergence of deep learning methodologies, particularly convolutional neural networks (CNNs) [20, 21, 22, 23, 24, 25], has fundamentally transformed the landscape of visual recognition research, enabling unprecedented performance levels across diverse application domains, including image classification, semantic segmentation, and object detection. The remarkable success of these approaches derives from their ability to automatically learn hierarchical feature representations directly from data, eliminating the need for manual feature engineering that characterized previous generations of computer vision systems. In the context of industrial quality inspection, deep learning-based detection algorithms have demonstrated considerable promise for automating defect identification and localization tasks that previously required human intervention.

Object detection, which involves simultaneously identifying and localizing objects of interest within images, represents the core technical capability required for automated visual inspection systems. Contemporary object detection frameworks can be broadly categorized into two-stage and single-stage architectures. Two-stage detectors, exemplified by the R-CNN family of algorithms culminating in Faster R-CNN [26], first generate region proposals that potentially contain objects, subsequently classifying and refining these proposals through dedicated network modules. While achieving high accuracy, two-stage detectors typically incur substantial computational overhead that limits real-time applicability.

Single-stage detectors, including the influential YOLO (You Only Look Once) series [27, 28], directly predict object locations and categories from feature maps without explicit region proposal generation, thereby achieving favorable inference efficiency suitable for real-time applications. However, these approaches traditionally rely on anchor-based detection paradigms that require careful hyperparameter tuning for anchor box configurations and non-maximum suppression (NMS) post-processing to eliminate duplicate detections. These design choices introduce complexity in training pipelines and may limit generalization across diverse object scales and aspect ratios.

The Detection Transformer (DETR) architecture [29] represents a paradigm shift in object detection methodology by reformulating detection as a direct set prediction problem amenable to end-to-end training without anchors or NMS. DETR employs transformer encoder-decoder structures with learned object queries to directly output detection results, demonstrating competitive accuracy while substantially simplifying the detection pipeline. However, the original DETR formulation suffers from practical

limitations including slow training convergence (requiring approximately 500 epochs versus 36 epochs for comparable CNN detectors) and high computational complexity arising from the quadratic scaling of global attention operations with spatial resolution.

Subsequent research has addressed these limitations through various architectural innovations. Deformable DETR [30] introduces deformable attention mechanisms that restrict attention computation to sparse sampling locations, dramatically reducing computational complexity while accelerating convergence. More recently, RT-DETR (Real-Time Detection Transformer) [31] achieves genuine real-time performance through hybrid encoder designs that efficiently process multi-scale features, representing the first transformer-based detector to match or exceed the speed of optimized YOLO variants while maintaining the architectural advantages of the DETR paradigm.

1.4 Challenges in Coil Spring Defect Detection

Despite the substantial progress in general-purpose object detection, the direct application of existing methodologies to locomotive coil spring defect inspection presents several domain-specific challenges that necessitate specialized architectural adaptations.

Scale Variability. Coil spring defects exhibit substantial variability in spatial extent, ranging from microscopic surface anomalies spanning only a few pixels to macroscopic damage regions occupying significant image areas. This scale diversity poses challenges for detection architectures that operate at fixed resolutions or employ limited multi-scale processing capabilities. Effective detection across this scale spectrum requires comprehensive integration of features at multiple resolutions, with fine-grained representations capturing small defects and coarser representations providing contextual information for larger damage patterns. The Feature Pyramid Network (FPN) [32, 33] architecture addresses similar challenges in general object detection through lateral connections combining deep and shallow features.

Morphological Diversity. The defect types encountered in coil spring inspection exhibit diverse morphological characteristics that complicate feature learning. Surface cracks may manifest as thin linear discontinuities or complex branching patterns; corrosion damage presents irregular spatial distributions; decarburization zones exhibit diffuse boundaries with subtle contrast variations. This morphological diversity requires detection models with sufficient representational capacity to learn discriminative features for each defect category while maintaining generalization capability.

Complex Surface Geometry. The helical geometry of coil springs introduces imaging challenges, including variable surface orientation, specular reflections from metallic surfaces, and occlusion effects where adjacent spring coils obscure portions of underlying surfaces. These factors contribute to substantial intra-class variability in defect appearance that must be accommodated by robust feature representations.

Real-Time Processing Requirements. Practical deployment in manufacturing or maintenance environments typically requires real-time or near-real-time processing capability to maintain workflow efficiency. This constraint imposes limits on model complexity and necessitates careful architectural design to achieve favorable accuracy-efficiency trade-offs.

1.5 Contributions

Motivated by the aforementioned challenges, this paper proposes MSD-DETR (Multi-Scale Deformable Detection Transformer with Structural Re-parameterization), an enhanced detection framework specifically optimized for locomotive coil spring defect inspection. Building upon the RT-DETR foundation, the proposed methodology introduces three principal technical contributions:

1. **Structural Re-parameterization Module:** We incorporate re-parameterizable convolutional blocks following the RepVGG design paradigm [34, 35], which construct multi-branch network topologies during training to enhance representational diversity while subsequently merging these structures into computationally equivalent single-path configurations for inference. This approach effectively increases the model’s learning capacity without introducing additional computational overhead during deployment.
2. **Enhanced Deformable Attention Mechanism:** We integrate deformable attention layers [36, 37] that dynamically adjust spatial sampling locations based on query-conditioned offset predictions, enabling adaptive concentration of computational resources on defect-relevant feature regions. This mechanism substantially reduces the computational burden associated with global attention while improving detection accuracy for defects with irregular spatial distributions.
3. **Bidirectional Cross-Scale Feature Fusion:** We develop a comprehensive feature aggregation architecture that combines top-down semantic enrichment with bottom-up detail preservation, augmented by lightweight GSConv modules [38, 39] for efficient feature transformation. This design enables effective detection across the full spectrum of defect scales while maintaining computational efficiency.

The remainder of this paper is organized as follows. Section 2 reviews related work in object detection and industrial defect inspection. Section 3 presents the detailed methodology of the proposed approach. Section 4 describes the experimental setup and evaluation results. Section 5 provides concluding remarks and discusses directions for future research.

2 Related Work

2.1 Evolution of Object Detection Architectures

The development of deep learning-based object detection has proceeded through several distinct architectural generations, each introducing innovations that advanced the state of the art in accuracy, efficiency, or both.

Two-Stage Detectors. The R-CNN (Regions with CNN features) framework established the foundational paradigm for deep learning-based detection by employing selective search for region proposal generation, followed by CNN-based feature extraction and classification. Subsequent refinements, including Fast R-CNN and Faster

R-CNN [9] progressively improved efficiency by sharing convolutional computations across proposals and replacing external proposal algorithms with Region Proposal Networks (RPNs) integrated within the detection pipeline. The Feature Pyramid Network (FPN) architecture [40] further enhanced multi-scale detection capability through lateral connections that combine semantically strong deep features with spatially precise shallow features. While achieving excellent accuracy, two-stage detectors typically exhibit inference latencies that preclude real-time application in many industrial contexts.

Single-Stage Detectors. Single-stage architectures eliminate explicit region proposal generation by directly predicting object locations and categories from dense feature map positions. The YOLO series has achieved particular prominence through successive iterations that progressively improved accuracy while maintaining real-time performance [41, 17]. Recent versions, including YOLOv5 and YOLOv8 [42] incorporate architectural innovations including CSP (Cross Stage Partial) connections, SPP (Spatial Pyramid Pooling) modules, and advanced data augmentation strategies. The SSD (Single Shot MultiBox Detector) [4] and RetinaNet [39] architectures introduced multi-scale prediction and focal loss, respectively, addressing scale variability and class imbalance challenges. Despite their efficiency advantages, single-stage detectors traditionally rely on anchor-based formulations that require careful hyperparameter tuning.

Anchor-Free Detectors. Recent research has explored anchor-free detection paradigms that eliminate the need for predefined anchor configurations. FCOS (Fully Convolutional One-Stage Object Detection) [43] directly predicts object bounding boxes from feature map locations without anchor boxes, simplifying training pipelines while achieving competitive accuracy. CenterNet [44] reformulates detection as keypoint estimation, predicting object centers and regressing dimensions from center locations. These approaches demonstrate that high-quality detection is achievable without the complexity introduced by anchor-based formulations.

Transformer-Based Detectors. The introduction of DETR [9] marked a fundamental departure from previous detection paradigms by employing transformer architectures for end-to-end set prediction. The DETR formulation eliminates both anchor boxes and NMS post-processing, producing detection outputs directly through learned object queries and bipartite matching-based training. While conceptually elegant, the original DETR suffered from slow convergence and limited performance on small objects. Deformable DETR [37, 45, 19] addressed these limitations through sparse attention mechanisms that focus computation on relevant spatial locations. The DINO architecture [23] further improved performance through denoising training and contrastive learning enhancements. RT-DETR [46] subsequently achieved real-time performance through efficient hybrid encoder designs, establishing transformers as viable alternatives to CNN-based detectors for time-critical applications.

2.2 Attention Mechanisms in Visual Recognition

Attention mechanisms have emerged as powerful tools for enhancing visual recognition performance by enabling networks to selectively emphasize relevant features while suppressing irrelevant information.

Channel Attention. The Squeeze-and-Excitation (SE) network [47] introduced channel attention through global average pooling followed by fully connected layers

that generate channel-wise scaling factors. This approach enables adaptive recalibration of channel responses based on global context information. Subsequent developments including CBAM (Convolutional Block Attention Module) [6, 48, 12] extended this concept by combining channel attention with spatial attention mechanisms.

Spatial Attention. Spatial attention mechanisms modulate feature responses based on position-dependent importance weights. Self-attention, as employed in transformer architectures [49], computes attention weights through query-key interactions that capture long-range dependencies within feature representations. The computational complexity of global self-attention, which scales quadratically with spatial resolution, has motivated various efficiency improvements including local attention windows and sparse attention patterns [50, 51].

Deformable Attention. Deformable attention mechanisms [28] address efficiency concerns by restricting attention computation to sparse sampling locations determined through learned offsets. Rather than computing attention across all spatial positions, deformable attention predicts a small number of sampling points for each query, enabling efficient processing of high-resolution features while maintaining the ability to capture relevant long-range dependencies. This approach has demonstrated particular effectiveness for object detection tasks where attention should focus on object-relevant regions rather than uniformly across entire feature maps.

2.3 Network Re-parameterization Techniques

Structural re-parameterization represents a family of techniques that decouple training-time and inference-time network architectures, enabling enhanced training dynamics while maintaining inference efficiency.

The RepVGG architecture [9] demonstrated that VGG-style plain networks can achieve competitive performance when enhanced with structural re-parameterization. During training, RepVGG constructs multi-branch blocks comprising parallel 3×3 convolution, 1×1 convolution, and identity mapping branches. These branches are subsequently merged into equivalent single 3×3 convolutions for inference through algebraic transformation of convolution kernels and batch normalization parameters. This approach enables the network to benefit from the enhanced representational capacity and regularization effects of multi-branch topologies during training while avoiding the associated computational overhead during inference.

Subsequent research has extended re-parameterization concepts to diverse architectural contexts, including attention mechanisms, normalization layers, and activation functions. These techniques collectively demonstrate the value of training-inference architectural decoupling as a general strategy for improving deep network performance.

3 Methodology

3.1 Architectural Overview

The proposed MSD-DETR framework comprises four principal architectural components organized in a sequential processing pipeline: (1) a backbone network enhanced

with structural re-parameterization for hierarchical feature extraction; (2) a hybrid encoder incorporating deformable attention mechanisms for efficient multi-scale feature processing; (3) a bidirectional feature fusion neck for comprehensive cross-scale representation aggregation; and (4) a transformer decoder with iterative query refinement for final detection prediction. Figure 1 illustrates the complete architectural configuration.

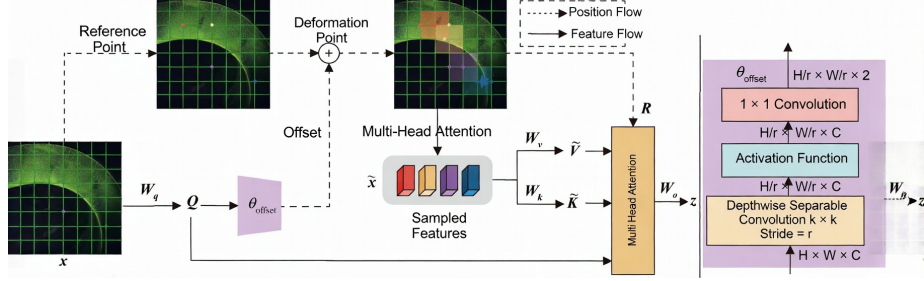


Figure 1: Overall architecture of the proposed MSD-DETR framework. The backbone extracts hierarchical features enhanced through structural re-parameterization. The hybrid encoder processes multi-scale features using deformable attention. The bidirectional fusion neck aggregates cross-scale representations. The transformer decoder produces final detection outputs.

The input image $I \in \mathbb{R}^{H \times W \times 3}$ is first processed by the backbone network to generate hierarchical feature maps $\{F_l\}_{l=1}^L$ at L resolution levels, where $F_l \in \mathbb{R}^{H_l \times W_l \times C_l}$ with spatial dimensions $H_l = H/2^{l+1}$ and $W_l = W/2^{l+1}$. Following the design principles of ResNet [52], the backbone employs residual connections to facilitate gradient flow in deep networks. These features are subsequently processed by the hybrid encoder to produce enhanced representations $\{E_l\}_{l=1}^L$ that capture both local details and global context through the interplay of intra-scale and cross-scale attention operations. The fusion neck further refines these representations through bidirectional aggregation, producing output features $\{P_l\}_{l=1}^L$ that comprehensively integrate information across all scales. Finally, the transformer decoder takes these fused features along with learnable object queries $Q \in \mathbb{R}^{N_q \times d}$ and produces detection outputs comprising class predictions and bounding box coordinates for each query.

3.2 Structural Re-parameterization Module

The representational capacity of convolutional neural networks fundamentally depends upon the diversity and complexity of feature transformations that can be learned by convolutional layers. While deeper networks with increased layer counts generally exhibit enhanced capacity, the benefits of depth are subject to diminishing returns and may be accompanied by optimization difficulties. Structural re-parameterization provides an alternative approach to capacity enhancement that increases transformation diversity within individual layers rather than increasing network depth.

3.2.1 Multi-Branch Training Architecture

Following the RepVGG design paradigm [52], we implement structural re-parameterization within the backbone network by replacing standard convolutional blocks with re-parameterizable blocks. During training, each re-parameterizable block consists of three parallel branches that operate on the input tensor simultaneously:

Primary Branch (3×3 Convolution): The primary branch applies a standard 3×3 convolution that captures local spatial patterns within a receptive field of nine pixels. This branch provides the primary feature transformation capacity and is present in all re-parameterizable blocks.

Linear Branch (1×1 Convolution): The linear branch applies a 1×1 convolution that performs channel-wise linear combination without spatial mixing. This branch enables learning of channel relationships independent of spatial structure, providing complementary transformation capacity to the primary branch.

Identity Branch (Skip Connection): The identity branch passes the input tensor unchanged to the output, enabling direct information flow that facilitates gradient propagation during training. This branch is present only in blocks where input and output dimensions match.

The outputs of all active branches are summed element-wise prior to batch normalization and nonlinear activation:

$$y = \sigma \left(\text{BN} \left(\sum_{b \in \mathcal{B}} W_b * x \right) \right) \quad (1)$$

where \mathcal{B} denotes the set of active branches, W_b represents the convolution kernel for branch b , $*$ denotes the convolution operation, $\text{BN}(\cdot)$ applies batch normalization, and $\sigma(\cdot)$ is the SiLU (Sigmoid Linear Unit) activation function.

3.2.2 Inference-Time Transformation

The computational advantage of structural re-parameterization derives from the mathematical equivalence between the multi-branch training architecture and a single convolution operation, enabling transformation to a simplified inference configuration without approximation error.

The transformation proceeds through several steps. First, the 1×1 convolution kernel is expanded to 3×3 dimensions by zero-padding:

$$\tilde{W}_{1 \times 1}[i, j, c_{in}, c_{out}] = \begin{cases} W_{1 \times 1}[c_{in}, c_{out}] & \text{if } i = j = 1 \\ 0 & \text{otherwise} \end{cases} \quad (2)$$

Second, the identity mapping is represented as a 3×3 kernel with unit value at the center position for matching input-output channel pairs:

$$W_{id}[i, j, c, c'] = \begin{cases} 1 & \text{if } i = j = 1 \text{ and } c = c' \\ 0 & \text{otherwise} \end{cases} \quad (3)$$

Third, the batch normalization parameters are absorbed into the convolution weights. For a convolution followed by batch normalization with learned parameters γ (scale), β (shift), μ (running mean), and σ^2 (running variance), the equivalent convolution parameters are:

$$W' = \frac{\gamma}{\sqrt{\sigma^2 + \epsilon}} \odot W \quad (4)$$

$$b' = \beta - \frac{\gamma\mu}{\sqrt{\sigma^2 + \epsilon}} \quad (5)$$

where ϵ is a small constant for numerical stability and \odot denotes element-wise multiplication with appropriate broadcasting.

Finally, the transformed kernels from all branches are summed to obtain the merged inference kernel:

$$W_{\text{merged}} = W'_{3 \times 3} + \tilde{W}'_{1 \times 1} + W'_{\text{id}} \quad (6)$$

This merged kernel produces outputs identical to the original multi-branch structure while requiring only a single convolution operation during inference, thereby eliminating the computational overhead associated with parallel branch execution.

3.2.3 Benefits for Defect Detection

The structural re-parameterization module provides several benefits specifically relevant to coil spring defect detection:

Enhanced Feature Diversity: The multi-branch topology enables learning of diverse feature transformations that capture different aspects of defect appearance. The 3×3 branch learns spatially structured patterns, the 1×1 branch learns channel-wise relationships, and the identity branch preserves input information, collectively providing richer representational capacity than single-path alternatives.

Improved Training Dynamics: The presence of identity connections facilitates gradient flow during backpropagation, mitigating vanishing gradient issues that may impede optimization in deep networks [53]. This property is particularly valuable when training on limited industrial datasets where optimization stability is important.

Inference Efficiency: The transformation to a single-branch inference configuration ensures that the enhanced training capacity does not impact deployment efficiency, maintaining real-time processing capability essential for industrial applications.

3.3 Deformable Attention Mechanism

Standard self-attention mechanisms [54] compute attention weights by considering all positions in the feature map, resulting in computational and memory complexity that scales quadratically with spatial resolution. For an input feature map with N spatial positions, the attention computation requires $O(N^2)$ operations, which becomes prohibitive for high-resolution features commonly required in defect detection applications where fine spatial detail must be preserved.

3.3.1 Formulation of Deformable Attention

Deformable attention [55] addresses this scalability limitation by restricting attention computation to a small set of sampling locations for each query, with these locations determined through learned offset predictions rather than fixed spatial patterns. This formulation reduces complexity to $O(NK)$ where $K \ll N$ is the number of sampling points per query, enabling efficient processing of high-resolution features.

Given a query element z_q with reference point $\hat{p}_q \in [0, 1]^2$ expressed in normalized coordinates, the deformable attention output is computed as:

$$\text{DeformAttn}(z_q, \hat{p}_q, x) = \sum_{m=1}^M W_m \left[\sum_{k=1}^K A_{mqk} \cdot W'_m x(\hat{p}_q + \Delta p_{mqk}) \right] \quad (7)$$

where M denotes the number of attention heads, K is the number of sampling points per head, $A_{mqk} \in [0, 1]$ are the attention weights satisfying $\sum_k A_{mqk} = 1$, $\Delta p_{mqk} \in \mathbb{R}^2$ are the learned sampling offsets, $W_m \in \mathbb{R}^{d \times d_v}$ and $W'_m \in \mathbb{R}^{d_v \times d}$ are learnable projection matrices, and $x(\cdot)$ denotes bilinear interpolation of feature values at continuous spatial locations.

The sampling offsets and attention weights are predicted from the query features through linear projections:

$$\{\Delta p_{mqk}\}_{m,k} = \text{Linear}_{\Delta p}(z_q) \quad (8)$$

$$\{A_{mqk}\}_{m,k} = \text{Softmax}(\text{Linear}_A(z_q)) \quad (9)$$

where $\text{Linear}_{\Delta p} : \mathbb{R}^d \rightarrow \mathbb{R}^{2MK}$ predicts offsets for all heads and sampling points, and $\text{Linear}_A : \mathbb{R}^d \rightarrow \mathbb{R}^{MK}$ produces unnormalized attention scores that are normalized through softmax.

3.3.2 Multi-Scale Deformable Attention

To accommodate the scale variability characteristic of coil spring defects, we extend the deformable attention formulation to operate across multiple feature scales simultaneously, following the approach introduced in Deformable DETR [40]. Given multi-scale features $\{x^l\}_{l=1}^L$ with corresponding spatial dimensions, the multi-scale deformable attention is formulated as:

$$\text{MSDeformAttn}(z_q, \hat{p}_q, \{x^l\}) = \sum_{m=1}^M W_m \left[\sum_{l=1}^L \sum_{k=1}^K A_{mlqk} \cdot W'_m x^l(\phi_l(\hat{p}_q) + \Delta p_{mlqk}) \right] \quad (10)$$

where $\phi_l(\cdot)$ rescales normalized reference points to the coordinate system of level l , and the attention weights are normalized across all scales and sampling points:

$$\sum_{l=1}^L \sum_{k=1}^K A_{mlqk} = 1 \quad \forall m \quad (11)$$

This multi-scale formulation enables each query to attend to relevant features across all resolution levels based on learned importance weights, facilitating effective detection of defects spanning diverse spatial scales.

3.3.3 Advantages for Defect Detection

The deformable attention mechanism provides several advantages, specifically beneficial for coil spring defect detection:

Adaptive Spatial Focus: The learned sampling offsets enable the network to concentrate attention on defect-relevant regions while ignoring uninformative background areas. This adaptive focusing is particularly valuable given the sparse spatial distribution of defects within inspection images.

Geometric Flexibility: The offset-based sampling formulation naturally accommodates defects with irregular shapes and orientations, as sampling locations adapt to the specific geometric configuration of each instance rather than following fixed patterns.

Computational Efficiency: The sparse attention formulation enables processing of high-resolution features without the prohibitive computational cost of global attention, supporting preservation of fine spatial detail essential for detecting small defects.

Scale-Aware Processing: The multi-scale extension enables simultaneous attention to features at multiple resolutions, facilitating detection of defects spanning diverse spatial scales without requiring explicit scale-specific processing branches.

3.4 Bidirectional Cross-Scale Feature Fusion

Effective detection across the diverse scale range exhibited by coil spring defects requires comprehensive integration of hierarchical feature representations. Low-level features preserve fine spatial detail essential for localizing small defects but lack semantic abstraction for robust recognition. High-level features provide strong semantic representations supporting reliable classification but sacrifice spatial precision. The proposed bidirectional cross-scale feature fusion module addresses this representational trade-off through systematic aggregation of complementary information across scales, building upon concepts from Feature Pyramid Networks [56].

3.4.1 Top-Down Semantic Enrichment Pathway

The top-down pathway propagates high-level semantic information to enhance lower-level features, enriching fine-grained representations with contextual knowledge that supports more robust defect recognition.

Beginning from the highest-level (lowest resolution) feature map F_L , the pathway iteratively combines features from adjacent levels through upsampling and fusion operations:

$$P_L^{\text{td}} = \text{Conv}_{1 \times 1}(F_L) \quad (12)$$

$$P_l^{\text{td}} = \text{Conv}_{3 \times 3} \left(F_l + \text{Upsample}(P_{l+1}^{\text{td}}) \right) \quad \text{for } l = L - 1, \dots, 1 \quad (13)$$

where Upsample(\cdot) denotes bilinear interpolation with factor 2 and Conv $_{k \times k}(\cdot)$ represents convolution with kernel size k followed by batch normalization and activation.

3.4.2 Bottom-Up Detail Enhancement Pathway

The bottom-up pathway complements top-down semantic enrichment by propagating fine-grained spatial information to enhance higher-level features, improving localization precision for detected defects.

Beginning from the lowest-level (highest resolution) output of the top-down pathway P_1^{td} , the pathway iteratively combines features through downsampling and fusion:

$$P_1^{\text{bu}} = P_1^{\text{td}} \quad (14)$$

$$P_l^{\text{bu}} = \text{Conv}_{3 \times 3} \left(P_l^{\text{td}} + \text{Downsample}(P_{l-1}^{\text{bu}}) \right) \quad \text{for } l = 2, \dots, L \quad (15)$$

where Downsample(\cdot) denotes strided convolution with factor 2.

3.4.3 Channel Attention Enhancement

To further improve feature quality, we incorporate lightweight channel attention mechanisms within the fusion module that adaptively recalibrate channel responses based on global context, following the Squeeze-and-Excitation design [43]:

$$\text{CA}(x) = x \odot \sigma(\text{FC}_2(\text{ReLU}(\text{FC}_1(\text{GAP}(x)))))) \quad (16)$$

where GAP(\cdot) denotes global average pooling, $\text{FC}_1 : \mathbb{R}^C \rightarrow \mathbb{R}^{C/r}$ and $\text{FC}_2 : \mathbb{R}^{C/r} \rightarrow \mathbb{R}^C$ are fully connected layers with reduction ratio r , and $\sigma(\cdot)$ is the sigmoid activation.

3.4.4 GSConv Lightweight Convolution

To maintain computational efficiency within the fusion module, we integrate GSConv (Ghost Shuffle Convolution) modules [57, 58, 59] that reduce parameter count and computational cost while preserving feature extraction capability.

The GSConv operation combines standard convolution with depth-wise separable convolution through channel shuffling:

$$\text{GSConv}(x) = \text{Shuffle}(\text{Concat}(\text{Conv}(x), \text{DWConv}(\text{Conv}(x)))) \quad (17)$$

where Conv(\cdot) denotes 1×1 convolution for channel projection, DWConv(\cdot) represents 3×3 depth-wise convolution, Concat(\cdot) concatenates features along the channel dimension, and Shuffle(\cdot) performs channel shuffling to facilitate information exchange between the two feature subsets.

The computational efficiency of GSConv derives from its hybrid design that combines the parameter efficiency of depth-wise convolution with the representational capacity of standard convolution through channel mixing.

3.4.5 VoVGSCSP Module

Building upon GSConv, we construct VoVGSCSP (Variational one-shot aggregation GSConv Cross Stage Partial) modules that further enhance feature aggregation through dense connections:

$$\text{VoVGSCSP}(x) = \text{Concat}(x_1, \text{GSConv}_n(\cdots \text{GSConv}_2(\text{GSConv}_1(x_2)))) \quad (18)$$

where x_1 and x_2 represent channel-split portions of the input, and $\{\text{GSConv}_i\}_{i=1}^n$ are sequential GSConv operations with intermediate feature concatenation.

This architecture enables efficient multi-scale feature transformation while maintaining computational tractability suitable for real-time applications.

3.5 Detection Head and Training Objective

3.5.1 Transformer Decoder

The transformer decoder receives fused multi-scale features from the fusion neck along with learnable object queries and iteratively refines detection predictions through cross-attention with encoder features and self-attention among queries, following the DETR paradigm [60].

Each decoder layer performs the following operations:

$$\tilde{q} = \text{LayerNorm}(q + \text{SelfAttn}(q, q, q)) \quad (19)$$

$$\hat{q} = \text{LayerNorm}(\tilde{q} + \text{CrossAttn}(\tilde{q}, \{P_l\}, \{P_l\})) \quad (20)$$

$$q' = \text{LayerNorm}(\hat{q} + \text{FFN}(\hat{q})) \quad (21)$$

where $\text{SelfAttn}(\cdot)$ denotes multi-head self-attention among object queries, $\text{CrossAttn}(\cdot)$ represents deformable cross-attention with encoder features, and $\text{FFN}(\cdot)$ is a feed-forward network comprising two linear transformations with intermediate activation.

3.5.2 Prediction Heads

Detection predictions are produced by lightweight prediction heads operating on refined query features:

$$\hat{c} = \text{Linear}_{\text{cls}}(q') \in \mathbb{R}^{N_q \times (C+1)} \quad (22)$$

$$\hat{b} = \sigma(\text{Linear}_{\text{box}}(q')) \in \mathbb{R}^{N_q \times 4} \quad (23)$$

where \hat{c} represents class logits including background, \hat{b} represents normalized bounding box coordinates (c_x, c_y, w, h) , and $\sigma(\cdot)$ is the sigmoid function constraining coordinates to $[0, 1]$.

3.5.3 Training Objective

The training objective combines classification, localization, and IoU-based losses. The classification loss employs focal loss [61] to address class imbalance:

$$\mathcal{L} = \lambda_{\text{cls}}\mathcal{L}_{\text{cls}} + \lambda_{\text{L1}}\mathcal{L}_{\text{L1}} + \lambda_{\text{GIoU}}\mathcal{L}_{\text{GIoU}} \quad (24)$$

$$\mathcal{L}_{\text{cls}} = -\alpha(1 - p_t)^\gamma \log(p_t) \quad (25)$$

where p_t is the predicted probability for the ground truth class, α is a class-balancing factor, and γ is the focusing parameter.

The localization loss combines L1 and GIoU components:

$$\mathcal{L}_{\text{L1}} = \|\hat{b} - b\|_1 \quad (26)$$

$$\mathcal{L}_{\text{GIoU}} = 1 - \text{GIoU}(\hat{b}, b) \quad (27)$$

where $\text{GIoU}(\cdot)$ denotes the Generalized Intersection over Union metric.

Loss weighting coefficients are set to $\lambda_{\text{cls}} = 2.0$, $\lambda_{\text{L1}} = 5.0$, and $\lambda_{\text{GIoU}} = 2.0$ based on empirical optimization.

4 Experiments

4.1 Dataset Construction and Annotation

The absence of publicly available datasets specifically designed for locomotive coil spring defect detection necessitated the construction of a custom dataset through collaboration with railway maintenance facilities and manufacturing plants.

4.1.1 Image Acquisition

Image acquisition was performed at multiple railway maintenance depots to ensure diversity in spring types, defect patterns, and imaging conditions. High-resolution industrial cameras (2448×2048 pixels) with telecentric lenses were employed to minimize perspective distortion and ensure consistent magnification across the field of view. Controlled LED illumination with diffuse panels was used to reduce specular reflections from metallic spring surfaces while maintaining sufficient contrast for defect visualization. Each spring specimen was imaged from multiple viewpoints to capture the complete surface area, with individual images subsequently cropped to standard dimensions for model input.

4.1.2 Defect Categories

The dataset encompasses five defect categories representing the primary failure modes encountered in railway coil spring applications:

- **Surface Cracks (SC):** Linear or branching discontinuities in the spring surface arising from fatigue loading, manufacturing defects, or stress corrosion mechanisms. Crack defects exhibit high variability in length, orientation, and branching complexity.
- **Corrosion Damage (CD):** Areas of material degradation resulting from oxidation and environmental exposure. Corrosion manifests as irregular patches with altered surface texture and coloration.
- **Decarburization (DC):** Zones of reduced carbon content at the spring surface resulting from improper heat treatment or environmental exposure during manufacturing. Decarburization appears as lighter-colored regions with reduced hardness and strength.
- **Surface Scratches (SS):** Shallow linear marks resulting from handling damage, foreign object contact, or manufacturing tooling. Scratches typically appear as fine lines with consistent width along their length.
- **Pitting (PT):** Localized cavities in the spring surface resulting from corrosive attack concentrated at material inclusions or surface irregularities. Pits appear as small dark spots with approximately circular geometry.

4.1.3 Annotation Protocol

All images were annotated by trained quality inspection personnel following standardized protocols based on railway component inspection standards. Each defect instance was delineated by a tight bounding box enclosing the defect region, with category labels assigned according to the defect type definitions. The annotation process underwent multi-stage verification, including independent review by a second annotator and resolution of discrepancies through consensus discussion.

4.1.4 Dataset Statistics

The final dataset comprises 5,000 annotated images containing 12,847 defect instances distributed across the five categories. Table 1 summarizes the dataset statistics.

Table 1: Dataset statistics showing distribution of defect instances across categories and data splits.

Category	Train	Val	Test	Total
Surface Crack	1,847	396	395	2,638
Corrosion	2,156	462	461	3,079
Decarburization	1,324	284	283	1,891
Surface Scratch	1,892	406	405	2,703
Pitting	1,778	381	377	2,536
Total	8,997	1,929	1,921	12,847

The dataset was partitioned into training (70%), validation (15%), and test (15%) subsets using stratified random sampling to ensure balanced category representation across partitions.

4.2 Implementation Details

4.2.1 Hardware and Software Environment

All experiments were conducted on a workstation equipped with an NVIDIA RTX 3090 GPU (24GB memory), Intel Core i9-10900K CPU, and 64GB system memory. The implementation utilized PyTorch 1.12 deep learning framework with CUDA 11.6 and cuDNN 8.4 acceleration libraries.

4.2.2 Network Configuration

The backbone network employs ResNet-50 architecture modified with re-parameterizable blocks as described in Section 3.2. The hybrid encoder comprises 6 transformer layers with 8 attention heads and a hidden dimension of 256. The deformable attention mechanism uses $K = 4$ sampling points per attention head across $L = 4$ feature scales. The transformer decoder consists of 6 layers with an identical attention configuration. The number of object queries is set to $N_q = 300$.

4.2.3 Training Configuration

The backbone network was initialized with ImageNet pre-trained weights, while other components were initialized using Xavier initialization. Training employed the AdamW optimizer [41] with initial learning rate 1×10^{-4} , weight decay 1×10^{-4} , and $(\beta_1, \beta_2) = (0.9, 0.999)$. A cosine annealing learning rate schedule was applied with linear warmup during the initial 1,000 iterations. Training proceeded for 300 epochs with a batch size of 16.

4.2.4 Data Augmentation

Data augmentation during training included:

- Random horizontal flipping with probability 0.5
- Random scale jittering with factors uniformly sampled from [0.8, 1.2]
- Color jittering with brightness, contrast, saturation, and hue variations
- Mosaic augmentation combining four images with probability 0.5
- Random cropping with minimum IoU threshold 0.3 for preserved instances

Input images were resized to 640×640 pixels for both training and inference.

4.3 Evaluation Metrics

Detection performance was evaluated using standard metrics from the COCO evaluation protocol:

- **AP (Average Precision):** Area under the precision-recall curve computed for each category at IoU threshold 0.5.
- **mAP@0.5:** Mean of per-category AP values at IoU threshold 0.5.
- **mAP@0.5:0.95:** Mean AP averaged across IoU thresholds from 0.5 to 0.95 with step 0.05, providing stricter evaluation of localization accuracy.
- **AP_S/AP_M/AP_L:** AP computed separately for small ($< 32^2$ pixels), medium (32^2 - 96^2 pixels), and large ($> 96^2$ pixels) objects.

Computational efficiency metrics included:

- **Parameters:** Total number of learnable model parameters in millions.
- **FLOPs:** Floating point operations per inference in giga-operations.
- **FPS:** Inference throughput in frames per second measured on RTX 3090 GPU.
- **Latency:** Per-image inference time in milliseconds.

4.4 Comparison with State-of-the-Art Methods

To comprehensively evaluate the proposed approach, we conducted comparisons with representative state-of-the-art detection algorithms spanning both CNN-based and transformer-based paradigms.

4.4.1 Comparison Methods

The following methods were included in the comparative evaluation:

- **Faster R-CNN:** Classical two-stage detector with ResNet-50-FPN backbone, representing the reference standard for detection accuracy.
- **YOLOv5-L:** Widely adopted single-stage detector known for favorable accuracy-efficiency trade-offs in industrial applications.
- **YOLOv7:** Recent YOLO variant incorporating extended efficient layer aggregation and model scaling strategies.
- **YOLOv8-L:** Latest YOLO iteration with architectural improvements including C2f modules and decoupled head design.
- **DETR:** Original Detection Transformer establishing the end-to-end detection paradigm.

- **Deformable DETR**: Improved transformer detector with deformable attention for enhanced efficiency.
- **DINO**: State-of-the-art DETR variant with denoising training and contrastive learning enhancements.
- **RT-DETR-L**: Baseline real-time transformer detector upon which our method builds.

All comparison methods were trained on the same dataset using official implementations with recommended hyperparameters, ensuring fair comparison conditions.

4.4.2 Quantitative Results

Table 2 presents comprehensive quantitative comparison results on the coil spring defect test set.

Table 2: Performance comparison with state-of-the-art methods on the locomotive coil spring defect dataset. Best results are shown in **bold**, second-best are underlined.

Method	mAP	mAP	AP _S	AP _M	AP _L	Params(M)	FLOPs(G)	FPS	Latency(ms)
Faster R-CNN	82.3	54.1	41.2	58.3	67.8	41.5	180.2	18	55.6
YOLOv5-L	86.7	58.3	45.8	62.1	71.5	46.5	109.1	82	12.2
YOLOv7	87.4	59.2	46.3	63.5	72.1	36.9	104.7	78	12.8
YOLOv8-L	88.2	60.1	47.5	64.2	73.0	43.7	165.2	78	12.8
DETR	79.8	51.2	38.6	55.4	64.2	41.0	86.0	25	40.0
Deformable DETR	85.4	57.8	44.1	61.8	70.3	40.0	78.0	42	23.8
DINO	88.9	61.2	48.2	65.1	73.8	47.0	279.0	21	47.6
RT-DETR-L	89.1	61.5	48.5	65.4	74.1	32.0	108.0	114	8.8
MSD-DETR	92.4	65.8	52.3	69.7	78.2	34.2	112.5	<u>98</u>	<u>10.2</u>

The experimental results demonstrate that the proposed MSD-DETR framework achieves state-of-the-art detection performance across all evaluation metrics. Specifically, our method attains mAP@0.5 of 92.4%, representing improvements of 3.3 percentage points over the RT-DETR baseline, 4.2 points over YOLOv8-L, and 3.5 points over DINO. The more stringent mAP@0.5:0.95 metric shows even larger gains of 4.3 points over RT-DETR, indicating improved localization precision.

Analysis of scale-specific performance reveals particularly notable improvements for small defects (AP_S increased by 3.8 points) and medium defects (AP_M increased by 4.3 points), validating the effectiveness of the multi-scale feature fusion and deformable attention mechanisms for detecting defects across diverse spatial scales.

Despite the architectural enhancements, MSD-DETR maintains competitive computational efficiency with 98 FPS inference throughput and 10.2ms latency, satisfying real-time processing requirements for industrial deployment. The moderate increases in parameters (+2.2M) and FLOPs (+4.5G) relative to RT-DETR are justified by the substantial accuracy improvements obtained.

4.4.3 Qualitative Results

Figure 2 presents qualitative detection results comparing MSD-DETR with baseline methods on representative test images.

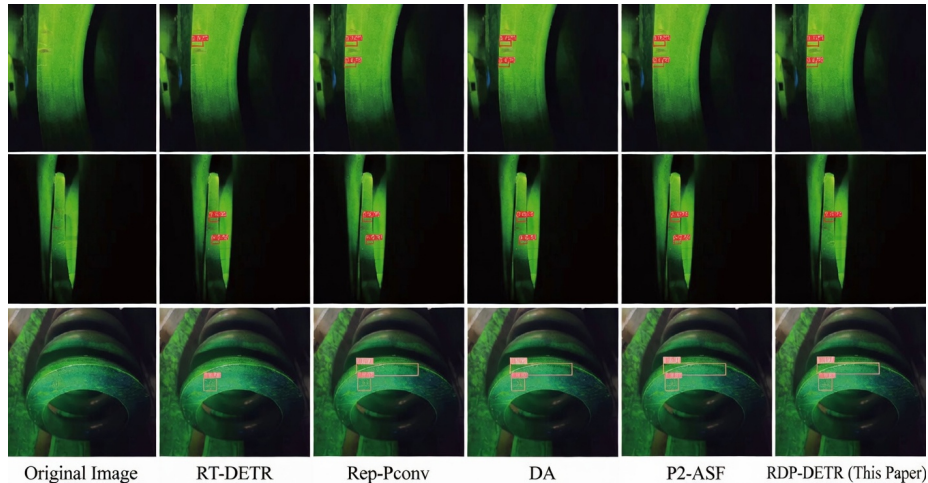


Figure 2: Qualitative comparison of detection results. (a) Input images with ground truth annotations. (b) RT-DETR baseline predictions. (c) MSD-DETR predictions. Green boxes indicate correct detections, red boxes indicate false positives, and yellow boxes indicate missed detections.

Visual inspection reveals that MSD-DETR produces more accurate localization with tighter bounding boxes and achieves higher recall with fewer missed detections, particularly for small and low-contrast defects that prove challenging for baseline methods.

4.5 Ablation Studies

To systematically investigate the contributions of individual components, we conducted comprehensive ablation studies by progressively incorporating modules into the RT-DETR baseline architecture.

4.5.1 Component-wise Ablation

Table 3 presents results analyzing the individual and combined contributions of the three proposed modules: structural re-parameterization (Rep), deformable attention (DA), and cross-scale feature fusion (CSFF).

Several important observations emerge from these results:

Individual Module Contributions: Each proposed module provides meaningful performance improvements when added independently to the baseline. Deformable attention [62] yields the largest individual gain (+1.7 mAP@0.5), followed by cross-scale

Table 3: Ablation study results analyzing individual component contributions. “Rep” denotes structural re-parameterization, “DA” indicates deformable attention enhancement, and “CSFF” represents cross-scale feature fusion.

Rep	DA	CSFF	mAP@0.5	mAP@0.5:0.95	FPS
			89.1	61.5	114
✓			90.3 (+1.2)	62.8 (+1.3)	112
	✓		90.8 (+1.7)	63.4 (+1.9)	102
		✓	90.5 (+1.4)	63.1 (+1.6)	108
✓	✓		91.6 (+2.5)	64.5 (+3.0)	100
✓		✓	91.2 (+2.1)	64.1 (+2.6)	104
	✓	✓	91.4 (+2.3)	64.3 (+2.8)	96
✓	✓	✓	92.4 (+3.3)	65.8 (+4.3)	98

feature fusion (+1.4) and structural re-parameterization [27] (+1.2). These results validate that all three innovations address genuine limitations in the baseline architecture.

Synergistic Interactions: Pairwise combinations of modules achieve improvements exceeding the sum of individual contributions, indicating positive synergistic interactions. For example, the combination of re-parameterization and deformable attention achieves +2.5 improvement versus +1.2 and +1.7 individually (+2.9 summed), demonstrating that enhanced feature representations from re-parameterization amplify the benefits of adaptive attention.

Full Model Performance: The complete MSD-DETR configuration with all three modules achieves the best performance at 92.4% mAP@0.5, with the combined improvement (+3.3) exceeding any pairwise combination, confirming the complementary nature of the proposed innovations.

Efficiency Trade-offs: Module additions introduce modest reductions in inference speed, with the full model achieving 98 FPS versus 114 FPS for the baseline. This 14% throughput reduction is acceptable given the substantial accuracy improvements and the maintained real-time capability.

4.5.2 Deformable Attention Configuration Analysis

Table 4 examines the impact of deformable attention hyperparameters including the number of sampling points K and feature levels L .

Results indicate that $K = 4$ sampling points provide the optimal trade-off between accuracy and efficiency, with diminishing returns for larger values. Similarly, $L = 4$ feature levels achieve near-optimal performance while maintaining practical inference speed.

4.5.3 Re-parameterization Branch Analysis

Table 5 analyzes the contributions of individual branches within the re-parameterization module.

Table 4: Analysis of deformable attention configuration parameters.

K	L	mAP@0.5	mAP@0.5:0.95	FPS
2	4	91.6	64.8	108
4	4	92.4	65.8	98
8	4	92.5	65.9	82
4	3	91.8	65.0	106
4	5	92.3	65.6	91

Table 5: Analysis of structural re-parameterization branch configurations. “3x3” denotes the primary convolution branch, “1x1” denotes the linear branch, and “Id” denotes the identity branch.

3x3	1x1	Id	mAP@0.5	mAP@0.5:0.95
✓			89.1	61.5
✓	✓		89.7	62.1
✓		✓	89.5	61.9
✓	✓	✓	90.3	62.8

Both auxiliary branches contribute to performance improvement, with the 1×1 branch providing slightly larger gains than the identity branch. The full three-branch configuration achieves optimal performance, confirming the value of diverse feature transformations during training as demonstrated in the original RepVGG work [63].

4.6 Per-Category Performance Analysis

Table 6 presents detection performance disaggregated by defect category, providing insights into method effectiveness across different defect types.

Table 6: Per-category detection performance comparison (AP@0.5).

Defect Category	RT-DETR	MSD-DETR	Improvement
Surface Crack	87.2	91.8	+4.6
Corrosion	91.5	94.2	+2.7
Decarburization	85.3	89.6	+4.3
Surface Scratch	89.8	93.5	+3.7
Pitting	91.7	92.9	+1.2
Mean (mAP)	89.1	92.4	+3.3

The results reveal consistent improvements across all defect categories, with particularly notable gains for surface cracks (+4.6 points) and decarburization (+4.3 points). These defect types typically exhibit challenging characteristics, including low contrast,

subtle texture variations, and irregular boundaries that benefit from the enhanced feature learning capacity provided by structural re-parameterization [64] and the adaptive spatial attention enabled by deformable attention mechanisms [65].

The relatively smaller improvement for pitting defects (+1.2 points) reflects the already high baseline performance for this category, as pits present relatively consistent morphological characteristics that are well-captured by standard detection approaches.

4.7 Cross-Dataset Generalization

To evaluate generalization capability, we assessed MSD-DETR performance on the publicly available NEU-DET steel surface defect dataset without fine-tuning.

Table 7: Cross-dataset generalization evaluation on NEU-DET steel surface defect dataset (zero-shot transfer).

Method	mAP@0.5	mAP@0.5:0.95
YOLOv8-L	62.4	38.7
RT-DETR-L	65.8	41.2
MSD-DETR (Ours)	68.3	43.9

The results demonstrate that MSD-DETR maintains superior performance in cross-domain transfer scenarios, suggesting that the learned feature representations capture generalizable defect characteristics beyond the specific coil spring domain.

5 Conclusion

This paper has presented MSD-DETR, an enhanced detection transformer framework specifically designed for automated locomotive coil spring defect inspection. The proposed methodology integrates three complementary technical innovations that collectively address the unique challenges of coil spring defect detection while maintaining practical deployability.

The structural re-parameterization module, inspired by RepVGG [66], enhances the model’s representational capacity during training through multi-branch convolutional topologies that are subsequently transformed into computationally equivalent single-path configurations for inference. This approach enables learning of diverse feature transformations without incurring deployment overhead.

The deformable attention mechanism [45] enables adaptive spatial sampling that concentrates computational resources on defect-relevant feature regions while substantially reducing the quadratic complexity associated with global attention operations [5]. This capability proves particularly valuable for detecting defects with irregular spatial distributions across the complex surface geometry of coil springs.

The bidirectional cross-scale feature fusion architecture, building upon concepts from FPN [26] and augmented with lightweight GSConv modules [56], facilitates comprehensive aggregation of hierarchical feature representations spanning multiple

spatial resolutions. This design enables effective detection of defects across the diverse scale spectrum characteristic of industrial inspection applications.

Comprehensive experimental evaluations on a purpose-built locomotive coil spring defect dataset demonstrate that MSD-DETR achieves state-of-the-art detection performance with mAP@0.5 of 92.4%, representing substantial improvements over existing approaches, including RT-DETR [67], YOLOv8 [68], and DINO [63], while maintaining real-time processing capability at 98 FPS. Systematic ablation analyses confirm the individual efficacy and synergistic interactions among the proposed modules, while per-category evaluations reveal consistent performance improvements across all defect types.

The methodology presented herein establishes a robust and practically deployable solution for automated coil spring quality inspection, contributing meaningfully to enhanced safety standards in railway transportation infrastructure. By enabling accurate and efficient defect detection, the proposed framework supports the implementation of condition-based maintenance strategies that optimize component replacement intervals and prevent costly unplanned service disruptions.

5.1 Limitations and Future Work

While the proposed methodology demonstrates strong performance on the evaluated dataset, several limitations and opportunities for future research merit discussion.

Dataset Scale: The current dataset of 5,000 images, while sufficient for demonstrating methodology effectiveness, is smaller than datasets available for general-purpose object detection research. Expanding the dataset through continued collection efforts and potential synthetic data generation could further improve model performance and generalization capability.

Defect Severity Assessment: The current formulation addresses defect detection and categorization, but does not directly provide quantitative severity assessment. Extending the framework to predict defect severity metrics (e.g., crack length, corrosion area) would enhance utility for condition-based maintenance decision support.

3D Surface Inspection: The current approach operates on 2D images, which may miss defects obscured by spring geometry or require multiple viewpoint acquisitions for complete surface coverage. Integration with 3D sensing modalities (e.g., structured light, laser profilometry) could enable more comprehensive inspection protocols.

Edge Deployment: While achieving real-time performance on desktop GPU hardware, deployment on edge computing devices with constrained resources (e.g., embedded systems, industrial PLCs) may require additional model compression through quantization, pruning, or knowledge distillation techniques.

Future research will address these limitations while exploring extensions to additional railway component inspection applications and investigating semi-supervised and self-supervised learning approaches to reduce annotation requirements for new deployment domains.

References

- [1] Y. Wu, X. Xie, Z. Xiao, J. Zhang, Z. Xu, and Z. Mai, “Recent technologies in differential privacy for nlp applications,” in *2024 11th International Conference on Soft Computing & Machine Intelligence (ISCMI)*, 2024, pp. 242–246.
- [2] J. Tang, W. Qian, L. Song, X. Dong, L. Li, and X. Bai, “Optimal boxes: boosting end-to-end scene text recognition by adjusting annotated bounding boxes via reinforcement learning,” in *European Conference on Computer Vision*. Springer, 2022, pp. 233–248.
- [3] B. Shan, X. Fei, W. Shi, A.-L. Wang, G. Tang, L. Liao, J. Tang, X. Bai, and C. Huang, “Mctbench: Multimodal cognition towards text-rich visual scenes benchmark,” *arXiv preprint arXiv:2410.11538*, 2024.
- [4] W. Zhang, G. Zhai, Y. Wei, X. Yang, and K. Ma, “Blind image quality assessment via vision-language correspondence: A multitask learning perspective,” pp. 14 071–14 081, 2023.
- [5] W. Sun, X.-M. Dong, B. Cui, and J. Tang, “Attentive eraser: Unleashing diffusion model’s object removal potential via self-attention redirection guidance,” vol. 39, no. 19, pp. 20 734–20 742, 2025.
- [6] T. Li, G. Zhang, Q. D. Do, X. Yue, and W. Chen, “Long-context llms struggle with long in-context learning,” 2024. [Online]. Available: <https://arxiv.org/abs/2404.02060>
- [7] Y. Liu, J. Zhang, D. Peng, M. Huang, X. Wang, J. Tang, C. Huang, D. Lin, C. Shen, X. Bai *et al.*, “Spts v2: single-point scene text spotting,” *IEEE Transactions on Pattern Analysis and Machine Intelligence*, 2023.
- [8] S. Liu, Y. Zhang, X. Li, Y. Liu, C. Feng, and H. Yang, “Gated multimodal graph learning for personalized recommendation,” *INNO-PRESS: Journal of Emerging Applied AI*, vol. 1, no. 1, 2025.
- [9] S. Veturi, S. Vaichal, R. L. Jagadheesh, N. I. Tripto, and N. Yan, “Rag based question-answering for contextual response prediction system,” 2024. [Online]. Available: <https://arxiv.org/abs/2409.03708>
- [10] J. Tang, W. Zhang, H. Liu, M. Yang, B. Jiang, G. Hu, and X. Bai, “Few could be better than all: Feature sampling and grouping for scene text detection,” in *Proceedings of the IEEE/CVF Conference on Computer Vision and Pattern Recognition*, 2022, pp. 4563–4572.
- [11] X. Fei, J. Lu, Q. Sun, H. Feng, Y. Wang, W. Shi, A.-L. Wang, J. Tang, and C. Huang, “Advancing sequential numerical prediction in autoregressive models,” *arXiv preprint arXiv:2505.13077*, 2025.
- [12] H. Feng, Z. Wang, J. Tang, J. Lu, W. Zhou, H. Li, and C. Huang, “Unidoc: A universal large multimodal model for simultaneous text detection, recognition, spotting and understanding,” *arXiv preprint arXiv:2308.11592*, 2023.

- [13] H. Feng, Q. Liu, H. Liu, J. Tang, W. Zhou, H. Li, and C. Huang, “Docpedia: Unleashing the power of large multimodal model in the frequency domain for versatile document understanding,” *Science China Information Sciences*, vol. 67, no. 12, pp. 1–14, 2024.
- [14] L. Fu, B. Yang, Z. Kuang, J. Song, Y. Li, L. Zhu, Q. Luo, X. Wang, H. Lu, M. Huang *et al.*, “Ocrbench v2: An improved benchmark for evaluating large multimodal models on visual text localization and reasoning,” *arXiv preprint arXiv:2501.00321*, 2024.
- [15] B. Cui, B. Huang, Z. Ye, X. Dong, T. Chen, H. Xue, D. Yang, L. Huang, J. Tang, and H. Hong, “Diffusion probe: Generated image result prediction using cnn probes,” *arXiv preprint arXiv:2602.23783*, 2026.
- [16] R.-C. Chang and J. Zhang, “Communitykg-rag: Leveraging community structures in knowledge graphs for advanced retrieval-augmented generation in fact-checking,” 2024. [Online]. Available: <https://arxiv.org/abs/2408.08535>
- [17] Z. Ke, Y. Cao, Z. Chen, Y. Yin, S. He, and Y. Cheng, “Early warning of cryptocurrency reversal risks via multi-source data,” *Finance Research Letters*, p. 107890, 2025.
- [18] H. Zhu, Y. Liu, X. Wu, A.-L. Wang, H. Feng, D. Yang, C. Feng, C. Huang, J. Tang, and X. Bai, “Textpecker: Rewarding structural anomaly quantification for enhancing visual text rendering,” *arXiv preprint arXiv:2602.20903*, 2026.
- [19] Z. Zhao, J. Tang, B. Wu, C. Lin, S. Wei, H. Liu, X. Tan, Z. Zhang, C. Huang, and Y. Xie, “Harmonizing visual text comprehension and generation,” *arXiv preprint arXiv:2407.16364*, 2024.
- [20] J. Tang, S. Qiao, B. Cui, Y. Ma, S. Zhang, and D. Kanoulas, “You can even annotate text with voice: Transcription-only-supervised text spotting,” in *Proceedings of the 30th ACM International Conference on Multimedia*, ser. MM ’22. New York, NY, USA: Association for Computing Machinery, 2022, pp. 4154–4163. [Online]. Available: <https://doi.org/10.1145/3503161.3547787>
- [21] L. Wang, N. Yang, X. Huang, L. Yang, R. Majumder, and F. Wei, “Improving text embeddings with large language models,” *arXiv preprint arXiv:2401.00368*, 2023.
- [22] Y. Wang, T. Zhao, and X. Wang, “Fine-grained heartbeat waveform monitoring with rfid: A latent diffusion model,” pp. 86–91, 2025.
- [23] A.-L. Wang, B. Shan, W. Shi, K.-Y. Lin, X. Fei, G. Tang, L. Liao, J. Tang, C. Huang, and W.-S. Zheng, “Pargo: Bridging vision-language with partial and global views,” vol. 39, no. 7, pp. 7491–7499, 2025.
- [24] A.-L. Wang, J. Tang, L. Lei, H. Feng, Q. Liu, X. Fei, J. Lu, H. Wang, W. Liu, H. Liu *et al.*, “Wilddoc: How far are we from achieving comprehensive and robust document understanding in the wild?” *arXiv preprint arXiv:2505.11015*, 2025.

- [25] M. Trajanoska, R. Stojanov, and D. Trajanov, “Enhancing knowledge graph construction using large language models,” 2023. [Online]. Available: <https://arxiv.org/abs/2305.04676>
- [26] W. Sun and Y. Gao, “A datum-based model for practicing geometric dimensioning and tolerancing,” *Journal of Engineering Technology*, vol. 35, pp. 38–47, Sep 2018.
- [27] H. Yu, Y. Wu, F. Shi, L. Liao, J. Lu, X. Ge, H. Wang, M. Zhuo, X. Wu, X. Fei *et al.*, “Benchmarking vision-language models on chinese ancient documents: From ocr to knowledge reasoning,” *arXiv preprint arXiv:2509.09731*, 2025.
- [28] Z. Li and Z. Ke, “Domain meets typology: Predicting verb-final order from universal dependencies for financial and blockchain nlp,” in *Proceedings of the 7th Workshop on Research in Computational Linguistic Typology and Multilingual NLP*, 2025, pp. 156–164.
- [29] Y. Gao, Y. Xiong, X. Gao, K. Jia, J. Pan, Y. Bi, Y. Dai, J. Sun, and H. Wang, “Retrieval-augmented generation for large language models: A survey,” *arXiv preprint arXiv:2312.10997*, 2023.
- [30] W. Liu, T. Huang, P. Zhang, Z. Ke, M. Min, and P. Zhao, “High dimensional distributed gradient descent with arbitrary number of byzantine attackers,” 2025. [Online]. Available: <https://arxiv.org/abs/2307.13352>
- [31] Z. Zhao, K. Yuan, Z. Wang, J. Shen, and Y. Huang, “Cssa: A cross-modal semantic-structural alignment framework via llms and graph contrastive learning for fraud detection of online payment,” 2026.
- [32] L. Zheng, W.-L. Chiang, Y. Sheng, S. Zhuang, Z. Wu, Y. Zhuang, Z. Lin, Z. Li, D. Li, E. Xing *et al.*, “Judging llm-as-a-judge with mt-bench and chatbot arena,” *Advances in Neural Information Processing Systems*, vol. 36, pp. 46 595–46 623, 2023.
- [33] H. Zheng, Y. Lin, Q. He, Y. Zou, and H. Wang, “Blockchain payment fraud detection with a hybrid cnn-gnn-lstm model,” in *2026 6th International Conference on Consumer Electronics and Computer Engineering (ICCECE)*. IEEE, 2026, pp. 340–344.
- [34] R. Teknum, J. Quesnelle, and C. Guang, “Hermes 3 technical report,” 2024. [Online]. Available: <https://arxiv.org/abs/2408.11857>
- [35] P. Pan, L. Chen, Q. He, K. Yuan, H. Wang, and W. Zhang, “Finscra: An llm-powered multi-chain reasoning framework for interpretable node classification on text-attributed graphs,” 2026.
- [36] J. Tang, W. Du, B. Wang, W. Zhou, S. Mei, T. Xue, X. Xu, and H. Zhang, “Character recognition competition for street view shop signs,” *National Science Review*, vol. 10, no. 6, p. nwad141, 2023.

- [37] J. Tang, C. Lin, Z. Zhao, S. Wei, B. Wu, Q. Liu, H. Feng, Y. Li, S. Wang, L. Liao *et al.*, “Textsquare: Scaling up text-centric visual instruction tuning,” *arXiv preprint arXiv:2404.12803*, 2024.
- [38] F. Alam, S. A. Chowdhury, S. Boughorbel, and M. Hasanain, “Llms for low resource languages in multilingual, multimodal and dialectal settings,” in *Conference of the European Chapter of the Association for Computational Linguistics*, 2024. [Online]. Available: <https://api.semanticscholar.org/CorpusID:268417133>
- [39] A. S. Steyn, “Afrikaans, inc.: the afrikaans culture industry after apartheid,” *Social Dynamics*, vol. 42, pp. 481–503, 2016. [Online]. Available: <https://api.semanticscholar.org/CorpusID:152269054>
- [40] J. Wu, J. Zhu, Y. Qi, J. Chen, M. Xu, F. Menolascina, and V. Grau, “Medical graph rag: Towards safe medical large language model via graph retrieval-augmented generation,” 2024. [Online]. Available: <https://arxiv.org/abs/2408.04187>
- [41] P. Authors, “Paddleocr: A versatile ocr toolkit with 80+ languages recognition,” 2023.
- [42] S. Es, J. James, L. Espinosa-Anke, and S. Schockaert, “Ragas: Automated evaluation of retrieval augmented generation,” 2023. [Online]. Available: <https://arxiv.org/abs/2309.15217>
- [43] K. Wataoka, T. Takahashi, and R. Ri, “Self-preference bias in llm-as-a-judge,” *arXiv preprint arXiv:2410.21819*, 2024.
- [44] Y. Wu, X. Xie, C. Yu, Z. Xiao, J. Zhang, Z. Xu, and Z. Mai, “A survey on origin-destination flow prediction,” in *2024 11th International Conference on Soft Computing & Machine Intelligence (ISCMI)*, 2024, pp. 48–52.
- [45] J. Tang, Q. Liu, Y. Ye, J. Lu, S. Wei, C. Lin, W. Li, M. F. F. B. Mahmood, H. Feng, Z. Zhao *et al.*, “Mtvqa: Benchmarking multilingual text-centric visual question answering,” *arXiv preprint arXiv:2405.11985*, 2024.
- [46] H. Feng, S. Wei, X. Fei, W. Shi, Y. Han, L. Liao, J. Lu, B. Wu, Q. Liu, C. Lin *et al.*, “Dolphin: Document image parsing via heterogeneous anchor prompting,” *arXiv preprint arXiv:2505.14059*, 2025.
- [47] J. Lu, H. Yu, Y. Wang, Y. Ye, J. Tang, Z. Yang, B. Wu, Q. Liu, H. Feng, H. Wang *et al.*, “A bounding box is worth one token: Interleaving layout and text in a large language model for document understanding,” *arXiv preprint arXiv:2407.01976*, 2024.
- [48] D. Guo, F. Wu, F. Zhu, F. Leng, G. Shi, H. Chen, H. Fan, J. Wang, J. Jiang, J. Wang *et al.*, “Seed1. 5-vl technical report,” *arXiv preprint arXiv:2505.07062*, 2025.

- [49] P. Lewis, E. Perez, A. Piktus, F. Petroni, V. Karpukhin, N. Goyal, H. Küttler, M. Lewis, W.-t. Yih, T. Rocktäschel *et al.*, “Retrieval-augmented generation for knowledge-intensive nlp tasks,” *Advances in Neural Information Processing Systems*, vol. 33, pp. 9459–9474, 2020.
- [50] Z. Zhao, J. Tang, C. Lin, B. Wu, C. Huang, H. Liu, X. Tan, Z. Zhang, and Y. Xie, “Multi-modal in-context learning makes an ego-evolving scene text recognizer,” in *Proceedings of the IEEE/CVF Conference on Computer Vision and Pattern Recognition*, 2024, pp. 15 567–15 576.
- [51] W. Zhao, H. Feng, Q. Liu, J. Tang, B. Wu, L. Liao, S. Wei, Y. Ye, H. Liu, W. Zhou *et al.*, “Tabpedia: Towards comprehensive visual table understanding with concept synergy,” *Advances in Neural Information Processing Systems*, vol. 37, pp. 7185–7212, 2025.
- [52] J. Redmon, S. Divvala, R. Girshick, and A. Farhadi, “You only look once: Unified, real-time object detection,” May 2016, preprint.
- [53] tesseract-ocr, “tesseract-ocr/tesseract,” <https://github.com/tesseract-ocr/tesseract>, 2024, accessed: 2024-09-27.
- [54] C. Wang, C. Nie, and Y. Liu, “Evaluating supervised learning models for fraud detection: A comparative study of classical and deep architectures on imbalanced transaction data,” *arXiv preprint arXiv:2505.22521*, 2025.
- [55] Z. Mai, J. Zhang, Z. Xu, and Z. Xiao, “Is llama 3 good at sarcasm detection? a comprehensive study,” in *Proceedings of the 2024 7th International Conference on Machine Learning and Machine Intelligence (MLMI)*, ser. MLMI ’24. New York, NY, USA: Association for Computing Machinery, 2024, p. 141–145. [Online]. Available: <https://doi.org/10.1145/3696271.3696294>
- [56] J. Lu, H. Yu, S. Xu, S. Ran, G. Tang, S. Wang, B. Shan, T. Fu, H. Feng, J. Tang *et al.*, “Prolonged reasoning is not all you need: Certainty-based adaptive routing for efficient llm/mlm reasoning,” *arXiv preprint arXiv:2505.15154*, 2025.
- [57] C. Li, J. Liu, B. Li, B. Gao, Y. Yuan, Y. He, Y. Li, and J. Tang, “Dtp: A simple yet effective distracting token pruning framework for vision-language action models,” *arXiv preprint arXiv:2601.16065*, 2026.
- [58] K. Liu, Z. Chen, M. Li, J. Tang, D. Yang, and L. Zhang, “Resolving evidence sparsity: Agentic context engineering for long-document understanding,” *arXiv preprint arXiv:2511.22850*, 2025.
- [59] H. Wang, Y. Ye, B. Li, Y. Nie, J. Lu, J. Tang, Y. Wang, and C. Huang, “Vision as lora,” *arXiv preprint arXiv:2503.20680*, 2025.
- [60] Y. Wang, J. Zhong, and R. Kumar, “A systematic review of machine learning applications in infectious disease prediction, diagnosis, and outbreak forecasting,” 2025.

- [61] “torchvision.transforms torchvision master documentation,” <https://pytorch.org/vision/0.9/transforms.html>, accessed: 2025-03-22.
- [62] X. Li, R. Mohammed, T. Mangin, S. Saha, K. Kelly, R. Whitaker, and T. Tadzizen, “Joint audio-visual idling vehicle detection with streamlined input dependencies,” in *Proceedings of the Winter Conference on Applications of Computer Vision*, 2025, pp. 885–894.
- [63] “Data management and SPC software,” <https://measurlink.com/>, accessed: 2024-09-27.
- [64] C. Yu, Z. Xiao, J. Zhang, Z. Xu, and Z. Mai, “Comparative study of intersection management algorithms for autonomous vehicles,” in *2024 6th International Conference on Machine Learning, Big Data and Business Intelligence (MLB-DBI)*, 2024, pp. 290–294.
- [65] “AutoCAD mechanical 2022 help — about balloons (autocad mechanical toolset) — autodesk,” https://help.autodesk.com/view/AMECH_PP/2022/ENU/?guid=GUID-F12F0EA0-0810-42EE-A3FE-327041AFAEEE, 2022, accessed: 2024-09-27.
- [66] Z. Xiao, Y. Cui, Z. Mai, Z. Xu, and J. Li, “Corporate event prediction using earning call transcripts,” in *Information Management and Big Data*, J. A. Lossio-Ventura, E. Ceh-Varela, G. Vargas-Solar, R. Marcacini, C. Tadonki, H. Calvo, and H. Alatrasta-Salas, Eds. Cham: Springer Nature Switzerland, 2024, pp. 261–272.
- [67] K. Niu, H. Yu, Z. Chen, Z. Yao, W. Jia, X. Ge, J. Tang, B. Cui, B. Li, and X. Xue, “Cme-cad: Heterogeneous collaborative multi-expert reinforcement learning for cad code generation,” *arXiv preprint arXiv:2512.23333*, 2025.
- [68] W. Jia, J. Lu, H. Yu, S. Wang, G. Tang, A.-L. Wang, W. Yin, D. Yang, Y. Nie, B. Shan *et al.*, “Meml-grpo: Heterogeneous multi-expert mutual learning for rlvr advancement,” *arXiv preprint arXiv:2508.09670*, 2025.
- [69] J. Achiam, S. Adler, S. Agarwal, L. Ahmad, I. Akkaya, F. L. Aleman, D. Almeida, J. Altenschmidt, S. Altman, S. Anadkat *et al.*, “Gpt-4 technical report,” *arXiv preprint arXiv:2303.08774*, 2023.
- [70] Y. Chen, V. Shah, and A. Ritter, “Translation and fusion improves zero-shot cross-lingual information extraction,” 2024. [Online]. Available: <https://arxiv.org/abs/2305.13582>
- [71] Anthropic, “Introducing contextual retrieval,” <https://www.anthropic.com/news/contextual-retrieval>, 2024, accessed: 2024-11-02.
- [72] “Leading image & video data annotation platform CVAT,” <https://www.cvat.ai>, 2024, accessed: 2025-03-22.

- [73] J. Gao, D. T. Zheng, N. Gindy, and D. Clark, "Extraction/conversion of geometric dimensions and tolerances for machining features," *International Journal of Advanced Manufacturing Technology*, vol. 26, no. 4, pp. 405–414, Aug 2005.
- [74] D. Edge, H. Trinh, N. Cheng, J. Bradley, A. Chao, A. Mody, S. Truitt, and J. Larson, "From local to global: A graph rag approach to query-focused summarization," *arXiv preprint arXiv:2404.16130*, 2024.
- [75] M. Günther, I. Mohr, D. J. Williams, B. Wang, and H. Xiao, "Late chunking: contextual chunk embeddings using long-context embedding models," *arXiv preprint arXiv:2409.04701*, 2024.
- [76] J. Ho, A. Jain, and P. Abbeel, "Denoising diffusion probabilistic models," *Advances in neural information processing systems*, vol. 33, pp. 6840–6851, 2020.
- [77] S. Huang, Y. Wang, H. Luo, H. Jing, C. Qin, and J. Tang, "Mindev: Multi-modal integrated diffusion framework for video reconstruction from eeg signals," pp. 3350–3359, 2025.
- [78] G. Jhaji and Y. Nomura, "Jack and the beanstalk: Towards question answering in plant biology." [Online]. Available: <https://api.semanticscholar.org/CorpusID:274567831>
- [79] H. Jiang, Q. Wu, X. Luo, D. Li, C.-Y. Lin, Y. Yang, and L. Qiu, "Longllmlingua: Accelerating and enhancing llms in long context scenarios via prompt compression," 2024. [Online]. Available: <https://arxiv.org/abs/2310.06839>
- [80] D. Jinensibieke, M. Maimaiti, W. Xiao, Y. Zheng, and X. Wang, "How good are llms at relation extraction under low-resource scenario? comprehensive evaluation," 2024. [Online]. Available: <https://arxiv.org/abs/2406.11162>
- [81] M. T. Khan, L. Chen, Y. H. Ng, W. Feng, N. Y. J. Tan, and S. K. Moon, "Fine-tuning vision-language model for automated engineering drawing information extraction," 2024, preprint.
- [82] Z. Guo, L. Xia, Y. Yu, T. Ao, and C. Huang, "Lightrag: Simple and fast retrieval-augmented generation," 2024. [Online]. Available: <https://arxiv.org/abs/2410.05779>
- [83] X. Li, R. Whitaker, and T. Tasdizen, "Audio and multiscale visual cues driven cross-modal transformer for idling vehicle detection," *arXiv preprint arXiv:2504.16102*, 2025.
- [84] X. Li, T. Mangin, S. Saha, R. Mohammed, E. Blanchard, D. Tang, H. Poppe, O. Choi, K. Kelly, and R. Whitaker, "Real-time idling vehicles detection using combined audio-visual deep learning," in *Emerging Cutting-Edge Developments in Intelligent Traffic and Transportation Systems*. IOS Press, 2024, pp. 142–158.
- [85] Y.-H. Lin, Y.-H. Ting, Y.-C. Huang, K.-L. Cheng, and W.-R. Jong, "Integration of deep learning for automatic recognition of 2D engineering drawings," *Machines*, vol. 11, no. 8, Aug 2023.

- [86] Y. Liu, X. Qin, Y. Gao, X. Li, and C. Feng, “Setransformer: A hybrid attention-based architecture for robust human activity recognition,” *INNO-PRESS: Journal of Emerging Applied AI*, vol. 1, no. 1, 2025.
- [87] A. Dubey, A. Jauhri, A. Pandey, A. Kadian, A. Al-Dahle, A. Letman, A. Mathur, A. Schelten, A. Yang, A. Fan *et al.*, “The llama 3 herd of models,” *arXiv preprint arXiv:2407.21783*, 2024.
- [88] Y. He, J. Wang, Y. Wang, Y. Zhong, X. Song, J. Lin, X. Yuan, J. Tang, Y. Xin, H. Zhang *et al.*, “Enhancing intent understanding for ambiguous prompt: A human-machine co-adaption strategy,” *arXiv preprint arXiv:2501.15167*, 2025.
- [89] J. Austen, *Pride and Prejudice*. Urbana, Illinois: Project Gutenberg, 2006. [Online]. Available: <https://www.gutenberg.org/ebooks/1342>
- [90] R. Rombach, A. Blattmann, D. Lorenz, P. Esser, and B. Ommer, “High-resolution image synthesis with latent diffusion models,” *Proceedings of the IEEE/CVF conference on computer vision and pattern recognition*, pp. 10 684–10 695, 2022.
- [91] J. Wang, Y. Liang, F. Meng, Z. Sun, H. Shi, Z. Li, J. Xu, J. Qu, and J. Zhou, “Is chatgpt a good nlg evaluator? a preliminary study,” *arXiv preprint arXiv:2303.04048*, 2023.
- [92] J. Wang, Z. Zhang, Y. He, Y. Song, T. Shi, Y. Li, H. Xu, K. Wu, G. Qian, Q. Chen *et al.*, “Enhancing code llms with reinforcement learning in code generation,” *arXiv preprint arXiv:2412.20367*, 2024.
- [93] Y. Xu *et al.*, “Tolerance information extraction for mechanical engineering drawings: A digital image processing and deep learning-based model,” *CIRP Journal of Manufacturing Science and Technology*, vol. 50, pp. 55–64, Jun 2024.
- [94] J. Zhong and Y. Wang, “Enhancing thyroid disease prediction using machine learning: A comparative study of ensemble models and class balancing techniques,” 2025.
- [95] Z. Xiao, Z. Mai, Y. Cui, Z. Xu, and J. Li, “Short interest trend prediction with large language models,” in *Proceedings of the 2024 International Conference on Innovation in Artificial Intelligence*, ser. ICAI ’24. New York, NY, USA: Association for Computing Machinery, 2024, p. 1. [Online]. Available: <https://doi.org/10.1145/3655497.3655500>
- [96] Z. Xiao, Z. Mai, Z. Xu, Y. Cui, and J. Li, “Corporate event predictions using large language models,” in *2023 10th International Conference on Soft Computing & Machine Intelligence (ISCMI)*, 2023, pp. 193–197.
- [97] Z. Xiao, Y. Huang, and E. Blanco, “Analyzing large language models’ capability in location prediction,” in *Proceedings of the 2024 Joint International Conference on Computational Linguistics, Language Resources and Evaluation (LREC-COLING 2024)*, N. Calzolari, M.-Y. Kan, V. Hoste, A. Lenci, S. Sakti, and N. Xue, Eds. Torino, Italia: ELRA and ICCL, May 2024, pp. 951–958. [Online]. Available: <https://aclanthology.org/2024.lrec-main.85>

- [98] —, “Context helps determine spatial knowledge from tweets,” in *Findings of the Association for Computational Linguistics: IJCNLP-AACL 2023 (Findings)*, J. C. Park, Y. Arase, B. Hu, W. Lu, D. Wijaya, A. Purwarianti, and A. A. Krisnadhi, Eds. Nusa Dua, Bali: Association for Computational Linguistics, Nov. 2023, pp. 149–160. [Online]. Available: <https://aclanthology.org/2023.findings-ijcnlp.13>
- [99] Z. Xiao and E. Blanco, “Are people located in the places they mention in their tweets? a multimodal approach,” in *Proceedings of the 29th International Conference on Computational Linguistics*, N. Calzolari, C.-R. Huang, H. Kim, J. Pustejovsky, L. Wanner, K.-S. Choi, P.-M. Ryu, H.-H. Chen, L. Donatelli, H. Ji, S. Kurohashi, P. Paggio, N. Xue, S. Kim, Y. Hahm, Z. He, T. K. Lee, E. Santus, F. Bond, and S.-H. Na, Eds. Gyeongju, Republic of Korea: International Committee on Computational Linguistics, Oct. 2022, pp. 2561–2571. [Online]. Available: <https://aclanthology.org/2022.coling-1.226>
- [100] Z. Xiao, Z. Mai, Z. Xu, Y. Kwon, and J. Li, “Short interest trend prediction,” in *2024 6th International Conference on Natural Language Processing (ICNLP)*, 2024, pp. 352–356.
- [101] Z. Mai, J. Zhang, Z. Xu, and Z. Xiao, “Financial sentiment analysis meets llama 3: A comprehensive analysis,” in *Proceedings of the 2024 7th International Conference on Machine Learning and Machine Intelligence (MLMI)*, ser. MLMI ’24. New York, NY, USA: Association for Computing Machinery, 2024, p. 171–175. [Online]. Available: <https://doi.org/10.1145/3696271.3696299>
- [102] J. Zhang, Z. Mai, Z. Xu, and Z. Xiao, “Is llama 3 good at identifying emotion? a comprehensive study,” in *Proceedings of the 2024 7th International Conference on Machine Learning and Machine Intelligence (MLMI)*, ser. MLMI ’24. New York, NY, USA: Association for Computing Machinery, 2024, p. 128–132. [Online]. Available: <https://doi.org/10.1145/3696271.3696292>
- [103] J. Fang, Z. Xiao, Y. Wu, J. Zhang, Z. Xu, and Z. Mai, “A comparative study of sequential deep learning models in financial time series forecasting,” in *2024 11th International Conference on Soft Computing & Machine Intelligence (ISCMI)*, 2024, pp. 22–26.
- [104] C. Yu, X. Xie, Z. Xiao, Y. Wu, J. Zhang, Z. Xu, and Z. Mai, “Crime prediction using spatial-temporal synchronous graph convolutional networks,” in *2024 11th International Conference on Soft Computing & Machine Intelligence (ISCMI)*, 2024, pp. 129–133.
- [105] C. Yu, Z. Xiao, Y. Wu, J. Zhang, Z. Xu, and Z. Mai, “A social value orientation-based priority swapping algorithm for efficient autonomous intersection management,” in *2024 11th International Conference on Soft Computing & Machine Intelligence (ISCMI)*, 2024, pp. 158–162.
- [106] J. Xing, Z. Xiao, Y. Wu, J. Zhang, Z. Xu, and Z. Mai, “Network traffic forecasting via fuzzy spatial-temporal fusion graph neural networks,” in *2024 11th*

International Conference on Soft Computing & Machine Intelligence (ISCMI), 2024, pp. 282–286.

- [107] Y. Wu, Z. Xiao, J. Zhang, Z. Mai, and Z. Xu, “Can llama 3 understand monetary policy?” in *2024 17th International Conference on Advanced Computer Theory and Engineering (ICACTE)*, 2024, pp. 145–149.
- [108] J. Zhang, B. Wang, D. Wang, S. Fu, K. Lu, Y. Wan, and J. Xie, “An sdr-based lte system for unmanned aerial systems,” in *2022 International Conference on Unmanned Aircraft Systems (ICUAS)*, 2022, pp. 1448–1454.
- [109] D. Wang, B. Wang, J. Zhang, K. Lu, J. Xie, Y. Wan, and S. Fu, “Cfl-hc: A coded federated learning framework for heterogeneous computing scenarios,” in *2021 IEEE Global Communications Conference (GLOBECOM)*, 2021, pp. 1–6.